

## POWDER CHARACTERIZATION AND OPTIMIZATION FOR ADDITIVE MANUFACTURING

**Laura Cordova<sup>1</sup>, Mónica Campos<sup>2</sup>, Tiedo Tinga<sup>1</sup>**

<sup>1</sup> UNIVERSITY OF TWENTE, Drienerlolaan 5, 7522 NB Enschede, Netherlands

<sup>2</sup> UNIVERSIDAD CARLOS III DE MADRID, Avda. Universidad, 30. 28911 Leganés,

e-mail: l.cordovagonzalez@utwente.nl

### ABSTRACT

Achieving the optimal quality for Additive Manufactured (AM) parts does not only depend on setting the right process parameters. Material feedstock also plays an important role when aiming for high performance products. The metal AM processes that are most applicable to industry, Powder Bed Fusion and Directed Energy Deposition, use metal powder as raw material. Therefore, controlling the quality and correctly characterizing the particles used in the process is a key step to successfully apply metal AM techniques. A correct flow of the powder and a constant apparent density over the build plate/substrate ensure a smooth process, less porosity and better surface resolution. In the present paper a methodology for AM powder characterization will be proposed, based on parameters like particle size distribution and shape, and experimental results will be presented. A series of representative materials from the above-mentioned techniques are studied to find the optimal particle parameters required in the metal AM processes.

**Key words:** Additive Manufacturing, Powder Bed Fusion (PBF), Directed Energy Deposition (DED), metal powders, image analysis, morphology, particle characterization

**Theme:** Metal powders for Additive Manufacturing

**Type of presentation:** oral

### 1 INTRODUCTION

A wide range of metal powders are commonly used as a feedstock for Additive Manufacturing (AM) techniques [1] such as Laser Beam Melting (LBM), Electron Beam Melting (EBM) and Directed Energy Deposition (DED). Metal Additive Manufacturing processes use a power source (e.g. laser or electron beam) to bind the particles through either a 'melting' or 'sintering' mechanism [2]. Similar to other Powder Metallurgy processes the particles play an important role for the mechanical properties of the parts [3, 4].

LBM and EBM belong to a group of AM techniques called Powder Bed Fusion (PBF) where the powder is applied in very thin layers and selectively melted with a laser or electron beam source, respectively. Alternatively, in the DED process the material is applied through a nozzle over the substrate. Some of the most significant parameters that determine the component quality produced by Powder

Bed Fusion processes are the laser power, laser scanning speed, thickness of the applied layer, diameter of the beam, hatching space and building direction. These group of features are directly linked to the amount of melted powder material involved when a part is built [5-7]. The average particle size for each metal AM technology varies. LBM requires the finest particles, ~35  $\mu\text{m}$  diameter on average, while for EBM this value is around 77  $\mu\text{m}$  and for DED the average ranges from 50-150  $\mu\text{m}$  [8-10].

This paper investigates specifically the particles role on the LBM process. The layer of powder applied over the build plate/substrate should be homogenous to ensure an optimal melting process. Layers that are too thin or too thick will result in poor mechanical properties due to overheating or lack of fusion. Therefore, the most critical parameters to study are the powder flowability and apparent density.

The particle size and morphology are key parameters for the correct flowability of particles during the LBM process. Particles smaller than 10 – 20  $\mu\text{m}$  can compromise the flowability. Also, spherical particles are desired to ensure a higher powder bed compaction. And finally, powder defects such as irregular shape, satellites and hollow particles should be avoided for a better distribution and less porosity [11]. Satellites are small powder grains stuck on the surface of a bigger particle. They can be formed either during the atomization process or when re-using the feedstock in the LBM machine. Further, some particles might contain internal porosity due to entrapped gas during the manufacturing process. This can result in lighter material with issues to flow. Furthermore, while the material is deposited over the build plate, the laser applies an homogenous amount of energy. If there is a high number of hollow particles this energy will not be homogeneously distributed.

## 2 MATERIALS AND METHODS

Four typical alloys used in the LBM process, as listed in Table 1, have been characterized with the objective of studying the influence of the particles morphology on the density and other features within the building process.

Table 1. Studied powdered materials

Nomenclature	Alloy system	Supplier
Inconel 718	Ni, Cr, Fe, Nb+Ta, Mo	Oerlikon
Ti6Al4V	Ti, Al, V	LPW Technology
Scalmalloy	Al, Mg, Sc	Airbus APWorks
AlSi10Mg	Al, Si, Mg	LPW

The density of the studied materials has been obtained by various methods. The first two values were calculated using the mixing rule (eq.1), and the expression for the theoretical pore free density (eq. 2), which yields the density of the true volume of the sintered material:

$$\rho = \sum w_i \cdot \rho_i \quad (1) \quad \rho' = \frac{1}{\sum (w_i / \rho_i)} \quad (2)$$

where,  $w_i$  is the weight fraction and  $\rho_i$  the density of the alloy component  $i$ .

Equation (1) was used to obtain  $\rho$  and  $\rho_{EDX}$ . The difference between them is that the first value takes as  $w_i$  the mass fractions provided by the powder manufacturer and the second is calculated with the wt. % estimated with Energy-

dispersive X-ray spectroscopy (EDX). Following the same argument,  $\rho'$  and  $\rho'_{EDX}$  were calculated with equation (2) considering the composition given by the supplier and estimated by EDX, respectively. And finally, the density was also measured with a Helium Gas Pycnometer (ASTM B923) [12], yielding the value  $\rho_{pycnometer}$ .

Using the standard Hall flowmeter method (ASTM B213) [13] the flow rate  $\Phi_{Hall}$  and apparent density  $\rho_{apparent}$  (ASTM B212) [14] were determined for all four powders. The particle size distribution was obtained with the Mastersizer 2000 (according to ASTM B 822-02) [15]. These experiments were carried out in a water based wet dispersion. In addition, to improve the sample dispersion and avoid agglomeration of powders, samples were placed in ultrasonic vibration for about 5-10 minutes before the measurements. Moreover, deflocculants as Fluicor PD 96/F and Dolapix CE64 were added to the suspension in order to improve the dispersion of Ti6Al4V and Inconel 718, respectively.

Finally, powder morphology was examined under the Keyence VHX-5000 digital microscope. Samples of each material were prepared by embedding the powder in epoxy resin and polishing. This facilitated the observation of the particles cross-sections under the microscope. The obtained data was also analyzed in terms of particle shape (i.e. aspect ratio) and circularity. Equations (3) and (4) define both parameters:

$$f_{shape} = \frac{minD}{maxD}; \{f_s \in \mathbb{Q} \mid 0 < f_s < 1\} \quad (3) \quad f_{circular} = \frac{4\pi A}{P^2}; \{f_c \in \mathbb{Q} \mid 0 < f_c < 1\} \quad (4)$$

where  $minD$  is the minimum particle diameter,  $maxD$  the maximum particle diameter,  $A$  the cross sectional area and  $P$  the perimeter of the particles.

### 3 RESULTS AND DISCUSSION

#### 3.1 Density

The density highly depends on the powder composition. Therefore, as the weight fraction of each element might vary across or even within the particles, it is important to know the average concentration. Table 4 shows a small deviation in the theoretical density due to variations of the composition (compare  $\rho$  vs  $\rho_{EDX}$  and  $\rho'$  vs  $\rho'_{EDX}$ ). The density value obtained with the pycnometer presents a somewhat larger error caused by the calibration and (limited) sample size.

Table 2. Density values

Material	$\rho$ (g/cm <sup>3</sup> )	$\rho'$ (g/cm <sup>3</sup> )	$\rho_{EDX}$ (g/cm <sup>3</sup> )	$\rho'_{EDX}$ (g/cm <sup>3</sup> )	$\rho_{pycnometer}$ (g/cm <sup>3</sup> )
Inconel 718	8.37	8.27	8.37	8.28	8.26
Ti6Al4V	4.35	4.27	4.36	4.28	4.38
Scalmalloy	2.69	2.65	2.64	2.62	2.68
AISI10Mg	2.65	2.65	2.64	2.63	2.65

#### 3.2 Particle Size Distribution (PSD)

Table 3 shows the obtained particle size distributions for the four studied powders, indicating the lower 10%, average and upper 10% particle sizes. The average particle size  $d(0.5)$  is very similar, around 35  $\mu\text{m}$ , except for

AlSi10Mg. Furthermore, Inconel 718 presents the narrowest distribution: from 23.90  $\mu\text{m}$  to 53.44  $\mu\text{m}$ , followed by Ti6Al4V. The two Al alloys have a wider size distribution. However, the applied laser diffraction method is more suitable for rounded particles as Inconel 718 and Ti6Al4V. As both Aluminum alloys have a more irregular morphology (to be discussed in the next subsection and Figure 1) the inaccuracy in the size distribution assessment might also be larger. As mentioned before, this characteristic (i.e. the PSD) influences the powder flowability and packing density. The apparent density (see Table 3), which was calculated with the mass deposited in a 25  $\text{cm}^3$  cup, presents variations in the four studied alloys. The maximum packing was obtained with Ti6Al4V and the minimum with AlSi10Mg. This phenomenon occurs due to differences in particle size distribution (Section 3.2) and morphology (Section 3.3). Ti6Al4V exhibited the most regular shape, which facilitates the packing. The flowability rate is largely influenced by the materials density. Despite the fact that the Hall method takes the same weight, 50g for every material, their volume is inversely proportional to the density. Therefore, Inconel 718 will always be the fastest one to flow, while AlSi10Mg will be the slowest.

Table 3. Particle size distribution (PSD)

Material	$d(0.1)$ ( $\mu\text{m}$ )	$d(0.5)$ ( $\mu\text{m}$ )	$d(0.9)$ ( $\mu\text{m}$ )	$\rho_{\text{apparent}}^*$ ( $\text{g}/\text{cm}^3$ )	$\Phi_{\text{Hall}}$ (g/s)
Inconel 718	23.90	35.84	53.44	4.36 (52.1%)	3.15
Ti6Al4V	22.18	35.14	55.29	2.38 (54.7%)	1.19
Scalmalloy	17.98	34.50	63.95	1.36 (50.5%)	0.67
AlSi10Mg	21.93	38.55	66.75	1.30 (49.1%)	0.52

(\*) The  $\rho_{\text{apparent}}$  (%) values were calculated dividing by the  $\rho$  (Table 2)

### 3.3 Morphology and porosity

Figure 1 shows the particles cross-sections. The images provide useful information such as internal porosity in the powders, morphology and estimated particle size distribution. Inconel 718 (Figure 1.a) shows an uniform and relatively round shape with some hollow particles. Ti6Al4V also presents very rounded particles and a uniform PSD. On the other hand, the particle shape of AlSi10Mg and Scalmalloy is less regular, internal porosity was higher and the PSD is not homogenous.

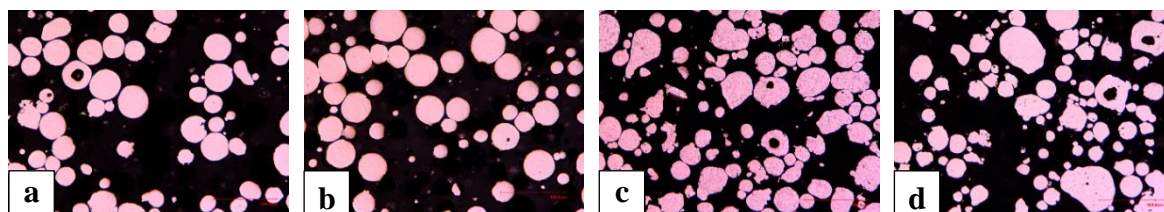


Figure 1. Powder cross-sections: a) Inconel 718, b) Ti6Al4V, c) AlSi10Mg, d) Scalmalloy

### 3.4 Morphological parameters of studied powders

The graphs in Figure 2 show a representation of the  $F_{\text{shape}}$  and  $F_{\text{circle}}$  parameters, which determine both the external regularity and how circular the particle is. This concept was applied before by [16, 17] to characterize the porosity obtained by a sintering process.

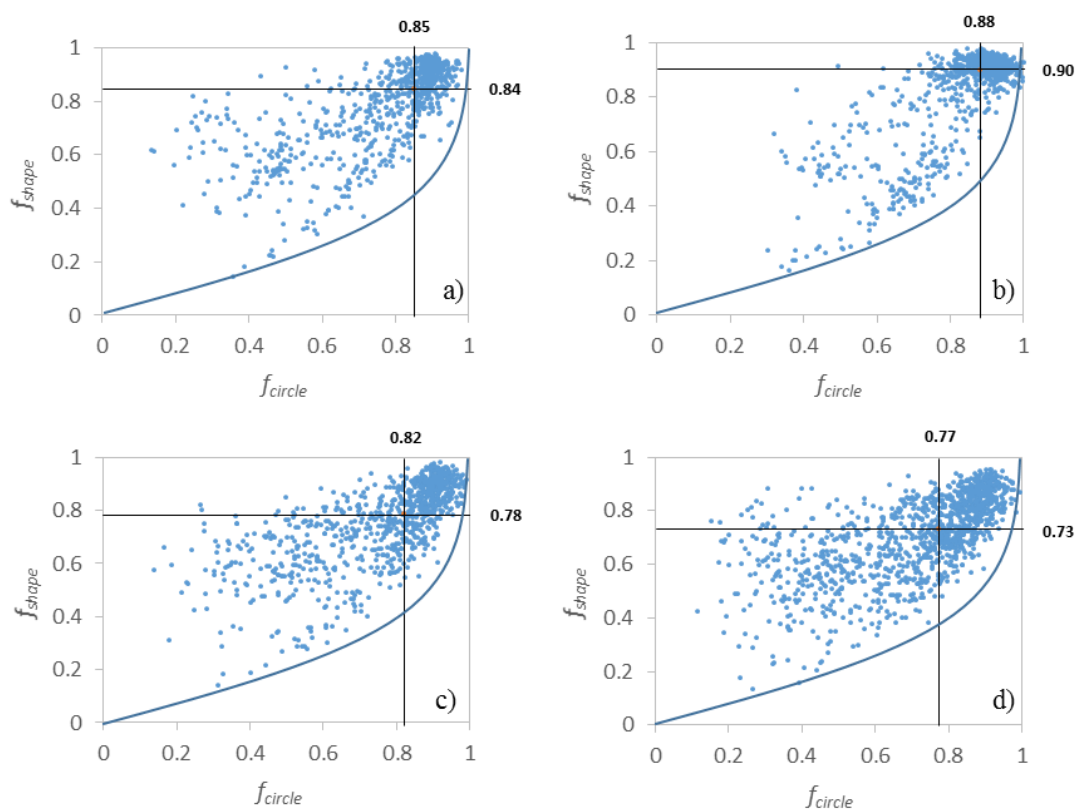


Figure 2.  $F_{circle}$  vs.  $F_{shape}$  form parameters for: a) Inconel 718, b) Ti6Al4V, c) Scalmalloy, d) AlSi10Mg

In Figure 2 the black lines represent the mean, which is the  $F_{shape}$  and  $F_{circle}$  value for 50% of the particles set. Ti6Al4V has the highest mean  $F_{shape}$  and  $F_{circle}$ , due to its regular morphology. This (i.e. morphology) has a large effect on the apparent density (Ti6Al4V presents a quite compact powder packing, see Table 3). Alternatively, AlSi10Mg presents, in general, lower values and more dispersion of  $F_{shape}$  and  $F_{circle}$ , mainly due to its surface irregularities and satellites.

#### 4 CONCLUSIONS

This study conducted with very different alloys, typically used for LBM, explains that to be able to correctly characterize AM metal feedstock, a complete assessment of the morphology, PSD and density has to be carried out. The information obtained helps to predict and understand the powder behavior over the build plate. In this investigation the powder that presented the most homogenous morphology with high  $F_{shape}$ ,  $F_{circle}$  parameters showed the highest apparent density values. On the contrary AlSi10Mg, with a wide PSD, irregular morphology and low  $F_{shape}$ ,  $F_{circle}$  values was the lowest in flowability rate and also apparent density.

#### ACKNOWLEDGMENTS

This research has been supported by the Netherlands Organization for Scientific Research under project number 438-13-207, named "Sustainability Impact of New Technology on After sales Service supply chains (SINTAS)". The authors would like to thank specially the Netherlands Aerospace Centre and Additive

Industries for their support during the experimental part of this research.

## REFERENCES

1. ISO Standard 17296-2, 2015 "Additive manufacturing: Overview of process categories and feedstock", Geneva, Switzerland, [www.iso.org](http://www.iso.org)
2. Kruth, J. P., P. Mercelis, J. Van Vaerenbergh, L. Froyen, and M. Rombouts, *Binding mechanisms in selective laser sintering and selective laser melting*. Rapid Prototyping Journal, 2005. **11**(1): p. 26-36.
3. J.M. Torralba, C. E. d. C., F. Velasco, *P/M aluminum matrix composites: an overview.pdf*. Journal of Materials Processing Technology 2003. **133**: p. 203–206.
4. Rahimian, M., N. Ehsani, N. Parvin, and H. r. Baharvandi, *The effect of particle size, sintering temperature and sintering time on the properties of Al–Al<sub>2</sub>O<sub>3</sub> composites, made by powder metallurgy*. Journal of Materials Processing Technology, 2009. **209**(14): p. 5387-5393.
5. Yadroitsev, I. and I. Smurov, *Selective laser melting technology: From the single laser melted track stability to 3D parts of complex shape*. Physics Procedia, 2010. **5**: p. 551-560.
6. Manfredi, D., F. Calignano, M. Krishnan, R. Canali, E. Ambrosio, and E. Atzeni, *From Powders to Dense Metal Parts: Characterization of a Commercial AlSiMg Alloy Processed through Direct Metal Laser Sintering*. Materials, 2013. **6**(3): p. 856.
7. Karlsson, J., A. Snis, H. Engqvist, and J. Lausmaa, *Characterization and comparison of materials produced by Electron Beam Melting (EBM) of two different Ti–6Al–4V powder fractions*. Journal of Materials Processing Technology, 2013. **213**(12): p. 2109-2118.
8. Zhao, X., S. Li, M. Zhang, Y. Liu, T. B. Sercombe, S. Wang, Y. Hao, R. Yang, and L. E. Murr, *Comparison of the microstructures and mechanical properties of Ti–6Al–4V fabricated by selective laser melting and electron beam melting*. Materials & Design, 2016. **95**: p. 21-31.
9. Gu, D. D., W. Meiners, K. Wissenbach, and R. Poprawe, *Laser additive manufacturing of metallic components: materials, processes and mechanisms*. International Materials Reviews, 2013. **57**(3): p. 133-164.
10. Kakinuma, Y., M. Mori, Y. Oda, T. Mori, M. Kashihara, A. Hansel, and M. Fujishima, *Influence of metal powder characteristics on product quality with directed energy deposition of Inconel 625*. CIRP Annals - Manufacturing Technology, 2016. **65**(1): p. 209-212.
11. Džugan, J. and Z. Novy, *Powder Application in Additive Manufacturing of Metallic Parts*. 2017.
12. ASTM Standard B 923 – 02, *Metal Powder Skeletal Density by Helium or Nitrogen Pycnometry*. ASTM International. West Conshohocken, PA, 2002.
13. ASTM Standard B213 – 03, 2003, "Flow Rate of Metal Powders", ASTM International, West Conshohocken, PA, [www.astm.org](http://www.astm.org)
14. ASTM Standard B212 – 99, *Apparent Density of Free-Flowing Metal Powders Using the Hall Flowmeter Funnel*. ASTM International. West Conshohocken, PA, 1999. **02.05**.
15. ASTM Standard B 822 – 02, 2002, "Particle Size Distribution of Metal Powders and Related Compounds by Light Scattering", ASTM International, West Conshohocken, PA, [www.astm.org](http://www.astm.org)
16. T. Marcu Puscas, M. S., A. Molinari, G. Straffellini, *Image analysis investigation of the effect of the process variables on the porosity of sintered chromium steels*. Materials Characterization, 2003. **50**(1): p. 1-10.
17. Mark L. Hentschel, N. W. P., *Selection of Descriptors for Particle Shape Characterization*. Part. Part. Syst. Charact. , 2003. **20**: p. 25 - 38.